Supporting Information for Impacts of Heteroatom Substitution on Excited State Dynamics of π-Extended Helicenes

Yuto Kondo,[a] Yusuke Tsutsui,[*a,b] Yusuke Matsuo,[a] Takayuki Tanaka,[*a] and Shu Seki[*a]

[a.] *Department of Molecular Engineering, Graduate School of Engineering, Kyoto University, Nishikyo-ku, Kyoto 615-8510, Japan*

[b.] *JST-PRESTO, Honcho 4-1-8, Kawaguchi, Saitama 332-0012, Japan*

1. Synthesis and characterization of compounds

General methods: ^{1}H- and ^{13}C-NMR were recorded with JEOL AL-400 (400 MHz for ^{1}H and 101 MHz for ^{13}C) and analyzed by ALICE and DELTA software. Chemical shifts were reported as the relative scale in ppm to internal standards $CHCl_3$ (δ = 7.26 ppm for ^{1}H, 77.16 ppm for ^{13}C) and acetone (δ = 2.05 ppm for ^{1}H, δ = 29.84 ppm for ^{13}C). Deuterated solvents were purchased from TCI and Aldrich (Merck) and noted for each compound. HR-APCI-TOF-MS spectra were taken with Thermo Fisher Scientific LTQ orbitrap XL model using positive mode. Single crystal of [9]TH was obtained from mixture solvent of $CHCl_3$/*n*-hexane. Single-crystal diffraction analysis data were collected at –180 °C with a Rigaku Saturn724+ CCD diffractometer with a graphite-monochromated Mo-Kα radiation (λ = 0.71073 Å). The structures were solved by direct methods (SHELXT-2018/2) and refined with full-matrix least squares technique (SHELXT-2018/3).

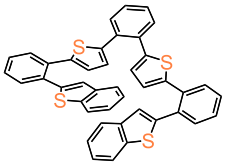

1

Procedure: A 200 mL three-neck round-bottom flask was charged with XPhos Pd G2 (78.6 mg, 0.10 mmol, 5.0 mol%), 1,2-bis(5-(2-bromophenyl)thiophen-2-yl)benzene (1.04 g, 2.0 mmol), and 2-(benzo[b]thiophen-2-yl)-4,4,5,5-tetramethyl-1,3,2-dioxaborolane (1.30 g, 5.0 mmol, 2.5 eq.). The reaction flask was evacuated and purged with argon three times. After the mixture was dissolved in dry THF (60 mL) and 0.5 M tripotassium phosphate solution (60 mL), the reaction mixture was stirred at room temperature for 24 h. After quenched with saturated aqueous ammonium chloride solution, the mixture was extracted with dichloromethane three times and the combined organic layers were washed with water and brine, and dried over anhydrous sodium sulfate. After removal of the solvents in vacuo, the residue was purified by column chromatography on silica with ethyl acetate/n-hexane (v/v = 1/6) as eluent gave **1** (396 mg, yield: 30%) as pale white solids.

^{1}H NMR (400 MHz, acetone-d_6) δ = 7.70 (m, 2H, benzo-H), 7.64–7.59 (m, 4H, benzo-H), 7.57–7.48 (m, 6H, benzo-H), 7.42 (m, 2H, benzo-H), 7.35 (m, 2H, benzo-H), 7.25–7.22 (m, 6H, benzo-H/thiophene-H), 6.78 (d, J = 3.4 Hz, 2H, thiophene-H), 6.68 (d, J = 3.4 Hz, 2H, thiophene-H) ppm.

^{13}C NMR (101 MHz, $CDCl_3$, room temperature) δ = 143.8, 143.5, 141.3, 140.6, 134.7, 134.5, 134.2, 132.0, 131.8, 131.6, 129.1, 128.7, 128.5, 128.1, 128.1, 124.8, 124.8, 124.4, 124.3, 122.7 ppm. (One peak is missing probably due to overlap)

HR-APCI-TOF-MS Found: *m/z* = 659.0994 $[M]^+$, calcd for $C_{42}H_{26}S_4$: *m/z* = 659.0990.

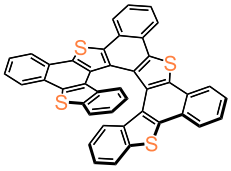

[9]TH

Procedure: A 300 mL three-necked round bottom flask was charged with **1** (340 mg, 0.50 mmol), DDQ (454 mg, 2.0 mmol, 4.0 eq.), and $Sc(OTf)_3$ (984 mg, 2.0 mmol, 4.0 eq.). The reaction flask was evacuated and purged with argon three times. After the mixture was dissolved in dry toluene (120 mL), and the resulting mixture was heated to reflux and kept for 3 h. After the mixture had been cooled to room temperature, the reaction mixture was diluted with chloroform and was passed through an alumina column with chloroform as the eluent. After evaporation of the solvent, the residue was further purified by recrystallization from chloroform to afford **[9]TH** (184 mg, yield: 55%) as yellow solids.

^{1}H NMR (400 MHz, $CDCl_3$) δ = 8.56 (dd, J_1 = 6.1 Hz, J_2 = 3.2 Hz, 2H, benzo-H), 8.44 (d, J = 7.8 Hz, 2H, benzo-H), 7.98 (d, J = 7.8 Hz, 2H, benzo-H), 7.83 (dd, J_1 = 6.1 Hz, J_2 = 3.2 Hz, 2H, benzo-H), 7.73 (td, J_1 = 7.4 Hz, J_2 = 1.1 Hz, 2H, benzo-H), 7.65 (td, J_1 = 7.4 Hz, J_2 =1.1 Hz, 2H, benzo-H), 7.58 (d, J = 8.3 Hz, 2H, benzo-H), 6.79 (td, J_1 = 7.4 Hz, J_2 = 1.1 Hz, 2H, benzo-H), 6.50 (d, J = 7.8 Hz, 2H, benzo-H), 5.86 (td, J_1 = 7.4 Hz, J_2 = 1.1 Hz, 2H, benzo-H) ppm.

^{13}C NMR (101 MHz, $CDCl_3$, room temperature) δ = 137.4, 135.4, 135.4, 135.3, 134.7, 130.8, 130.0, 129.3, 127.9, 127.4, 127.3, 126.9, 126.8, 125.3, 125.1, 124.9, 124.9, 123.1, 121.4, 121.1 ppm. (One peak is missing probably due to overlap)

HR-APCI-TOF-MS Found: *m/z* = 653.0524 $[M+H]^+$, calcd for $C_{42}H_{21}S_4$: *m/z* = 653.0521.

NMR Spectra

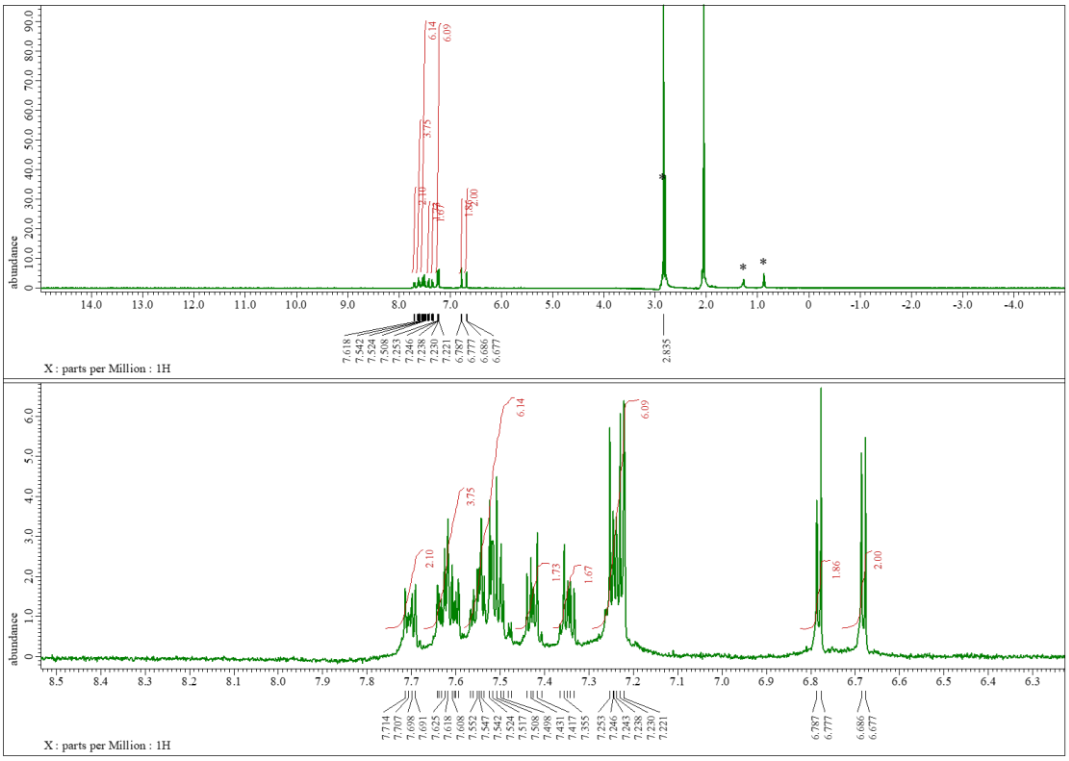

Fig. S1-1 ^{1}H NMR spectrum of **1** in acetone-d_6 at room temperature. Peaks with * are due to the residual solvents.

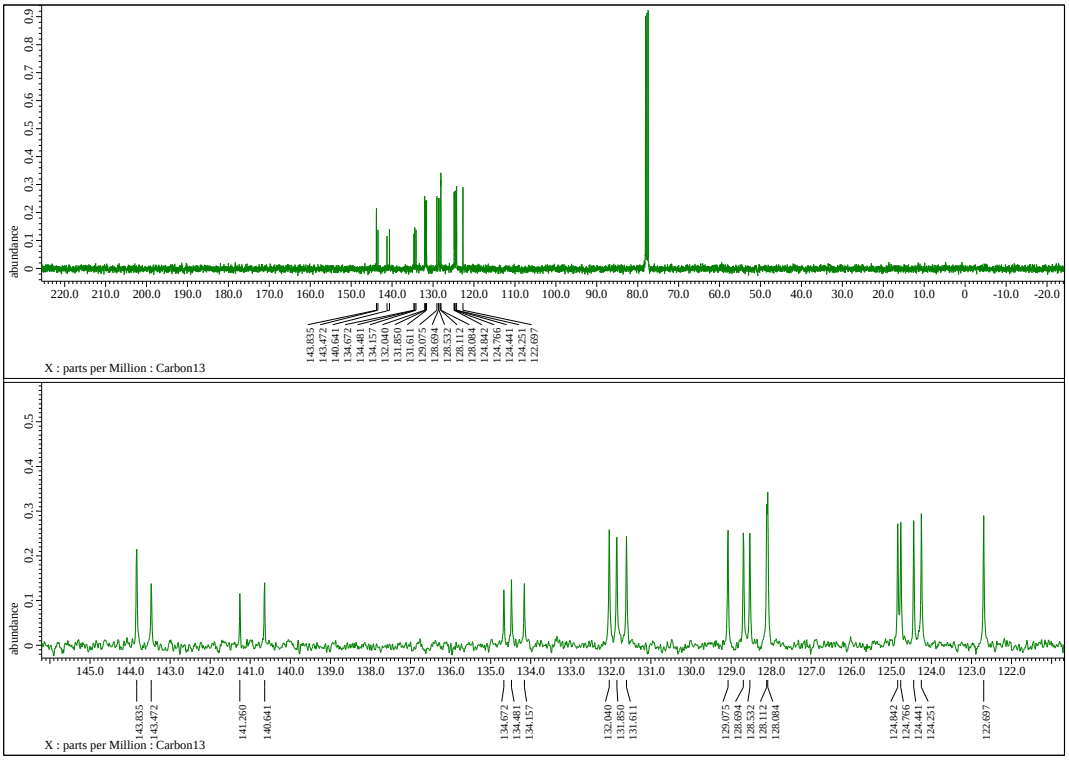

Fig. S1-2 ^{13}C NMR spectrum of **1** in $CDCl_3$ at room temperature.

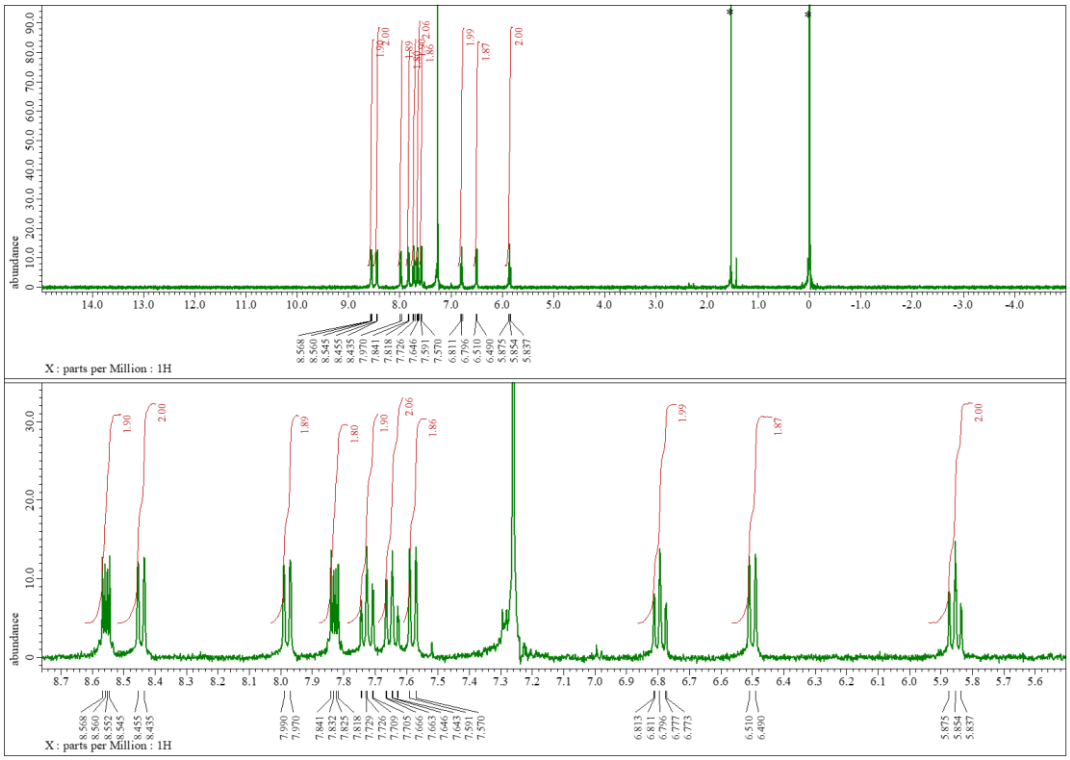

Fig. S1-3 ^{1}H NMR spectrum of **[9]TH** in $CDCl_3$ at room temperature. Peaks with * are due to the residual solvents.

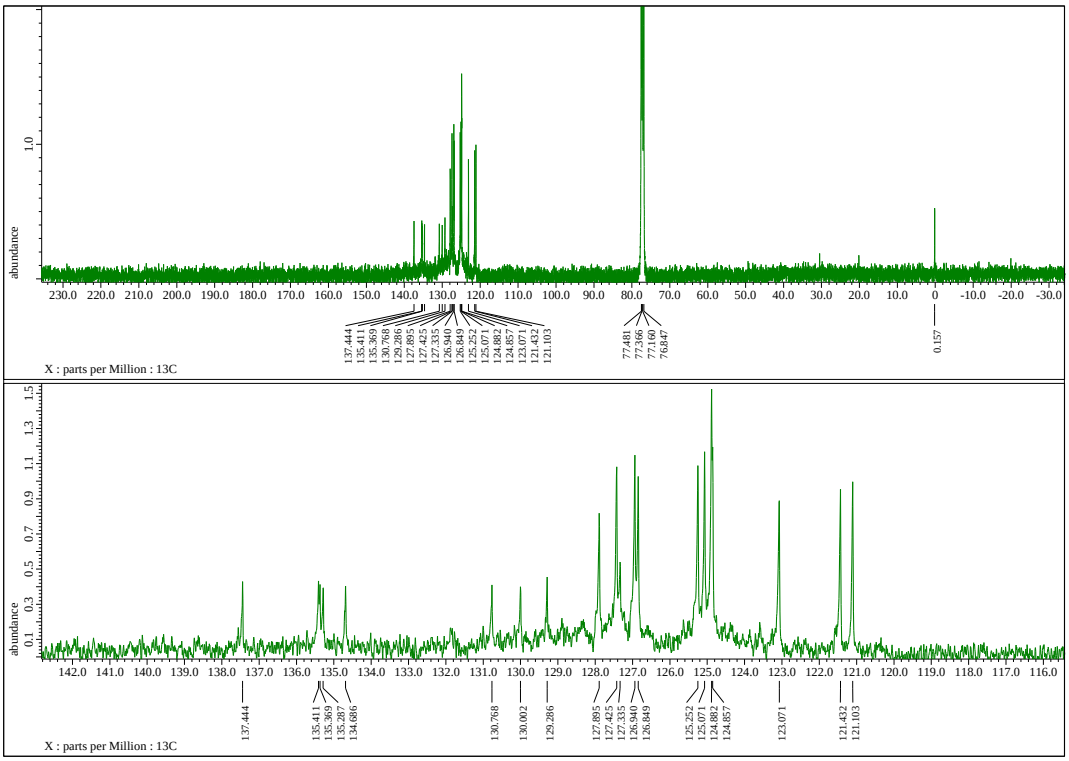

Fig. S1-4 ^{13}C NMR spectrum of **[9]TH** in $CDCl_3$ at room temperature.

Mass Spectra

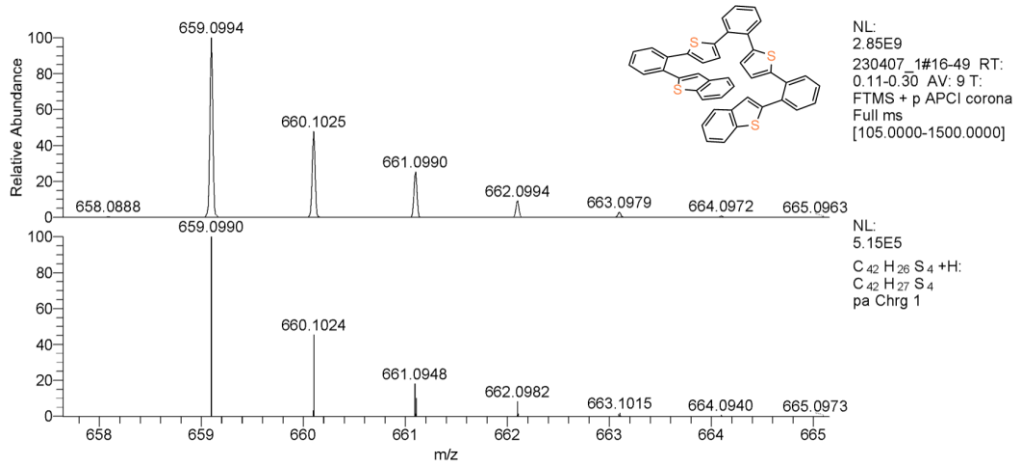

Fig. S1-5 HR-APCI-TOF-mass spectra of **1**. (Top; observed. Bottom; calculated [*M*+H]$^+$.)

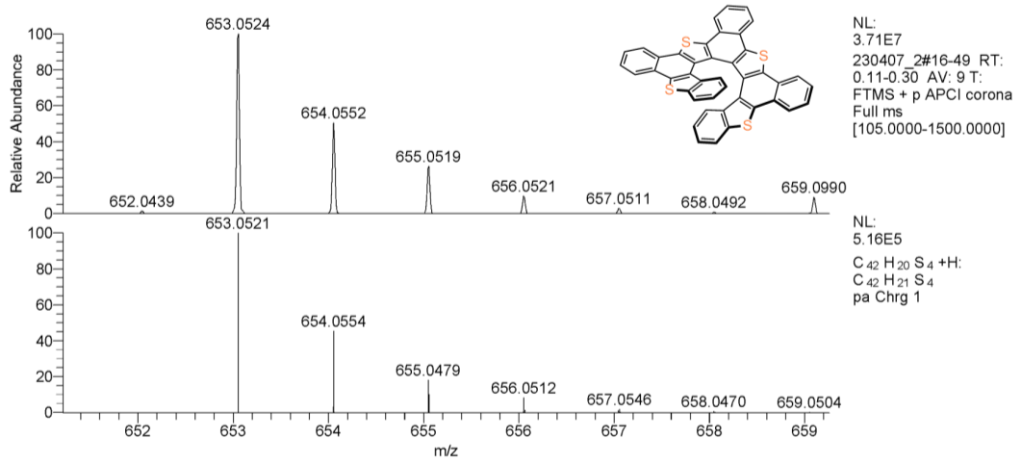

Fig. S1-6 HR-APCI-TOF-mass spectra of **[9]TH**. (Top; observed. Bottom; calculated [*M*+H]$^+$.)

X-Ray Crystallographic Details

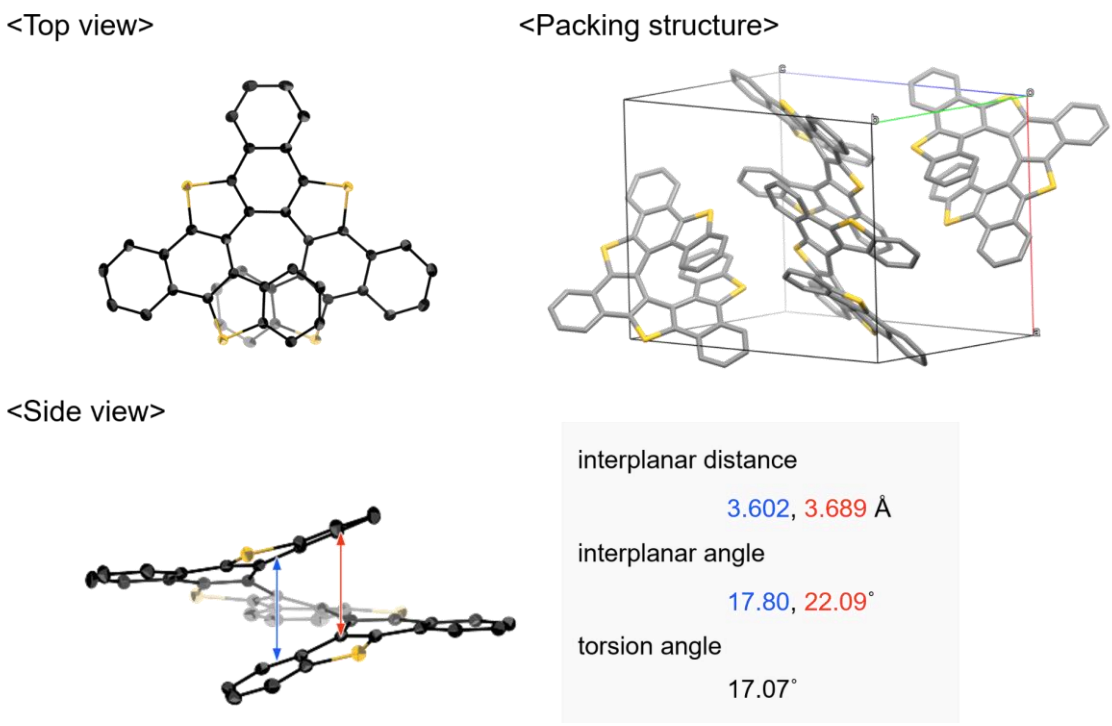

Fig. S1-7 X-Ray crystal structure of **[9]TH**. Thermal ellipsoids were scaled to 50% probability. (left) Top view and side view. (right) Packing structure. Hydrogen atoms are omitted for clarity.

Table S1-1. Crystal data and structure refinements for **[9]TH**.

Compound	**[9]TH**
Empirical Formula	$C_{42}H_{20}S_4$
M_W	652.82
Crystal System	Monoclinic
Space Group	$P2_1/c$ (No. 14)
a [Å]	13.0508(3)
b [Å]	13.0701(4)
c [Å]	16.2937(5)
α [deg]	90
β [deg]	91.738(3)
γ [deg]	90
Volume [Å^3]	2913.42(14)
Z	4
Density [g/cm^3]	1.488
Completeness	1.000
Goodness-of-fit	1.039
R_1 [$I > 2\sigma(I)$]	0.0391
wR_2 (all data)	0.1040
Solvent System	$CHCl_3$/*n*-hexane
CCDC No.	2311848

2. Cyclic voltammetry and electrochemically induced absorption spectra of [9]TH

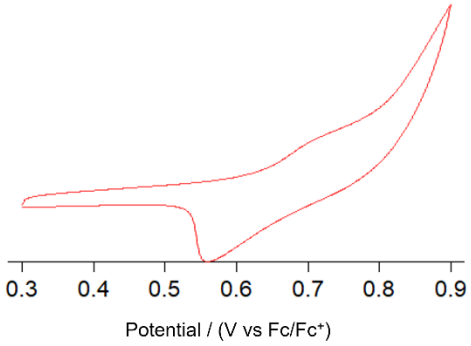

Fig. S2 Cyclic voltammogram of **[9]TH** in tetrahydrofuran.

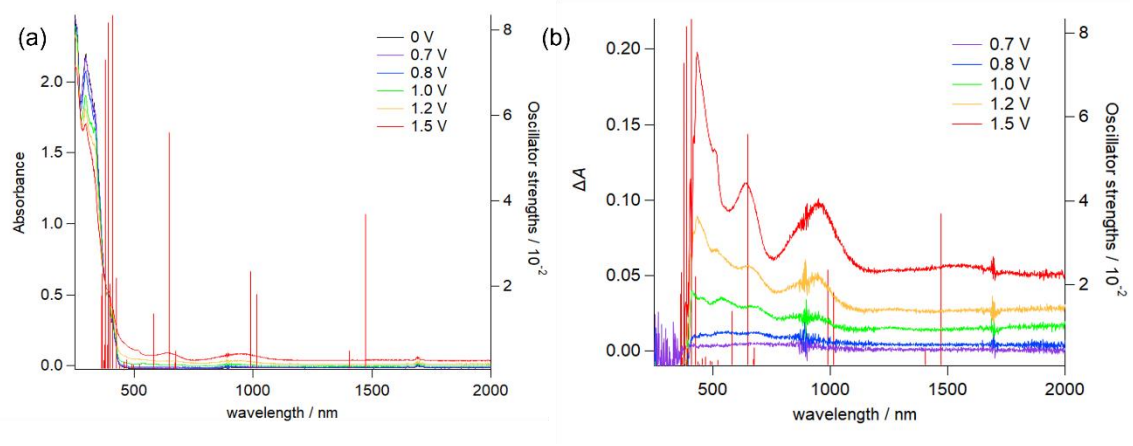

Fig. S3 (a) Electrochemically induced absorption of **[9]TH** in dichloromethane. (b) Same as (a) represented as differential absorption. Red bars indicate theoretically estimated oscillator strength of the radical cation.

3. Chiral separation, CD, and CPL spectra of [9]TH

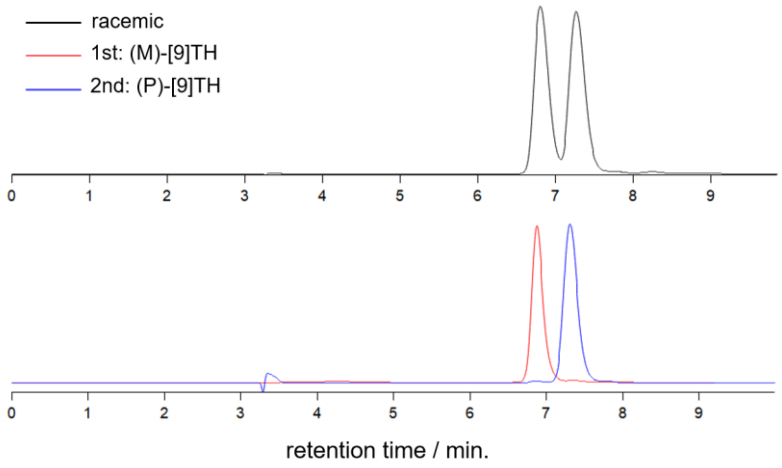

Fig. S4 Chiral HPLC separation of **[9]TH** eluted by dichloromethane/*n*-hexane (v/v = 0.25/0.75) with a flow rate of 1.0 mL/min (SUMICHIRAL OA-3100).

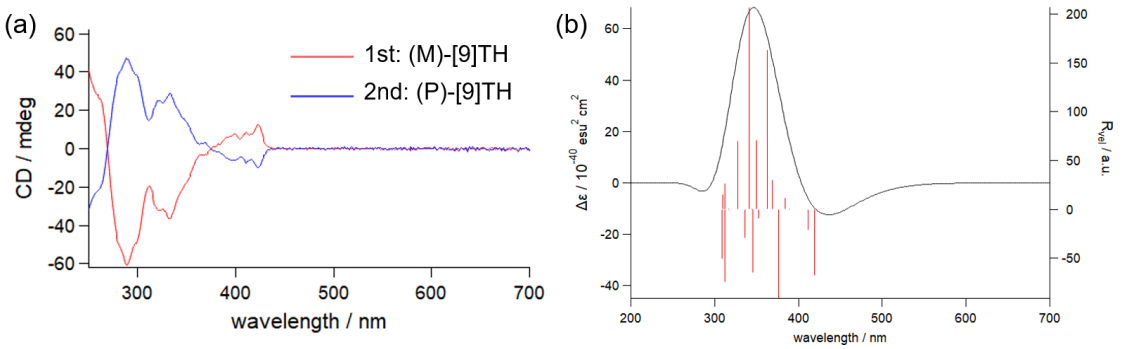

Fig. S5 (a) Circular dichroism spectra of **[9]TH** of the first (red) and second (blue) fraction shown in Fig. S4. (b) Simulated ECD spectra suggesting (P)-**[9]TH** corresponds to the 2nd fraction.

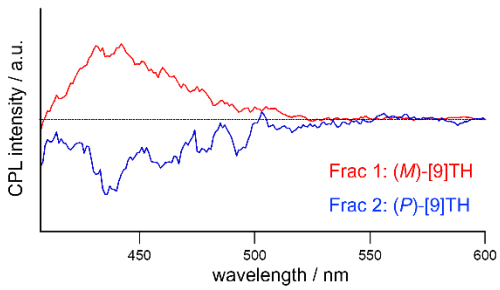

Fig. S6 Circularly polarized luminescence (CPL) spectra from [9]TH in dichloromethane under the excitation at 350 nm.

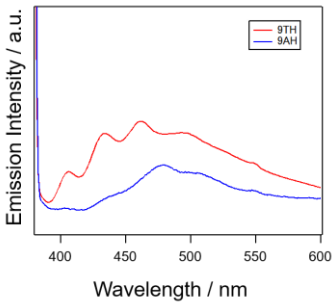

Fig. S7 Emission spectra of drop casted films of 9TH (red) and 9AH (blue) under the excitation at 370 nm."

4. Additional data for transient absorption spectroscopy

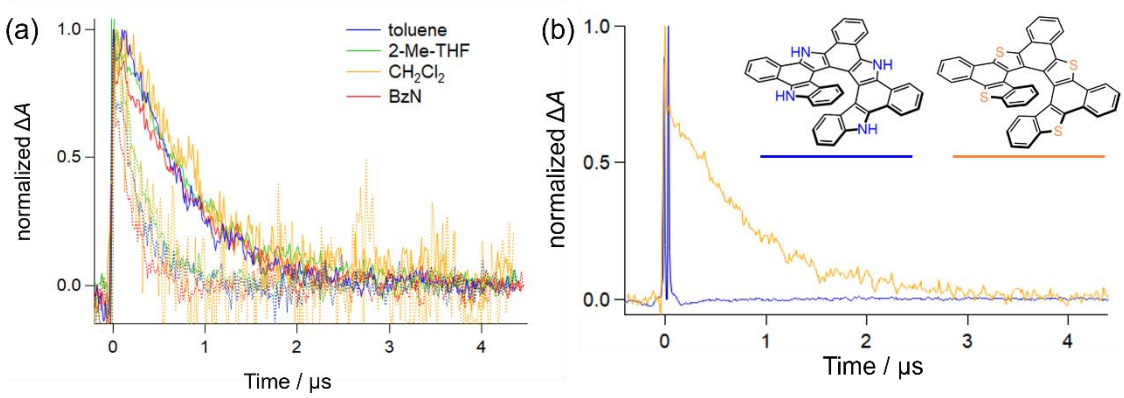

Fig. S8 (a) Transient absorption traces of **[9]TH** at 480 nm in various solvents. Solid and dotted lines represent N_2 saturated and O_2 saturated conditions, respectively. (b) Transient absorption of **[9]TH** (orange) and **[9]AH** (blue) at 480 nm in 2-methyltetrahydrofuran. The prompt response is the contribution from fluorescence.

Table S2 Decay constants τ in μs for transient absorption traces of **[9]TH** at 480 nm in various solvents.

Solvent	Under N_2	O_2 bubbled
Toluene	0.66	0.27
CH_2Cl_2	0.74	0.24
Benzonitrile	0.83	0.19
2-Me-THF	0.84	0.31

For all solvents, the decay constants reduced under O_2 bubbled condition.

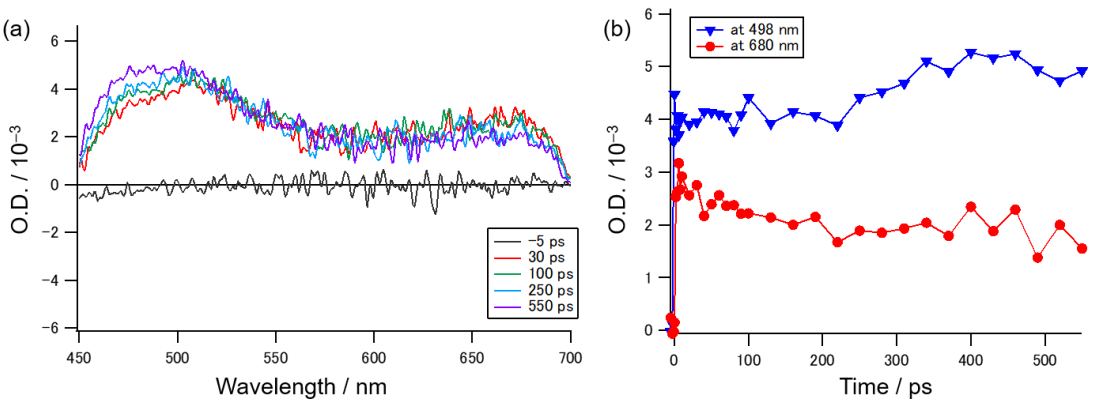

Fig. S9 (a) Picosecond transient absorption spectra and (b) kinetics of **[9]TH** in dichloromethane.

Picosecond transient absorption spectra was obtained as follows. Around 60 fs pulses from

Ti:Sapphire regenerative amplifier was frequency doubled into 400 nm by a BBO crystal and used as pump pulses with the excitation energy of 1 mW. A small portion of the fundamental was fed into a sapphire plate to generate supercontinuum for probe pulses. These pulses were focused and non-collinearly overlapped with a small angle to the sample, which is dissolved in dichloromethane with 10^{-3} M. Dispersion was corrected with a polynomial fitting.

5. Time-resolved photoluminescence spectroscopy

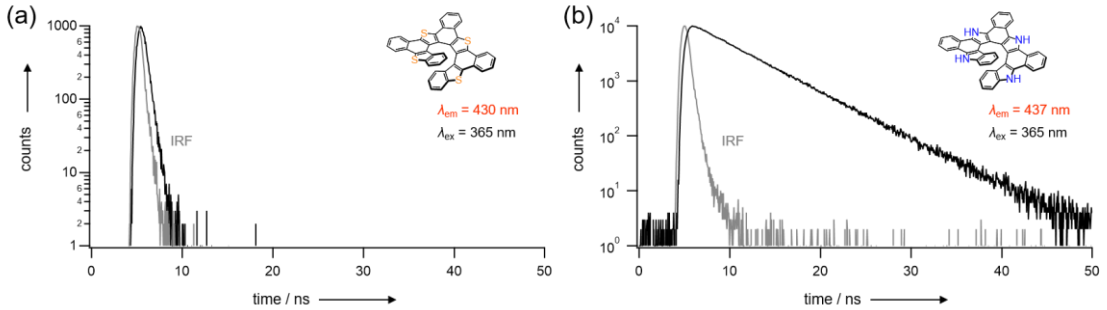

Fig. S10 Time resolved photoluminescence from (a) **[9]TH** and (b) **[9]AH** in dichloromethane at room temperature. Gray lines represent instrumental response functions (IRF).

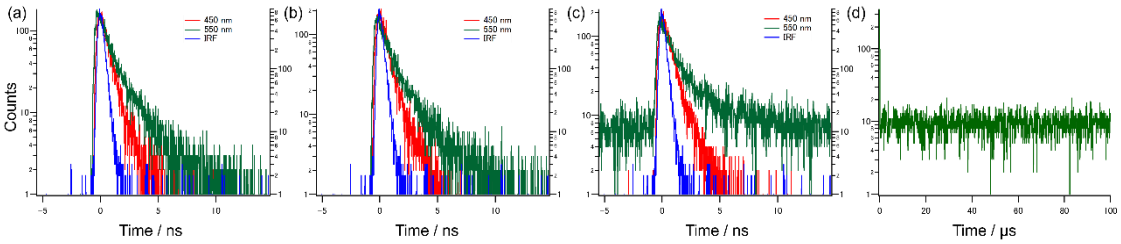

Fig. S11 Time resolved photoluminescence from **[9]TH** in 2-Me-THF at (a) −120°C, (b) −150°C, and (c, d) −190°C. Excitation pulses were at 405 nm and a band-pass filter was used for emission at 450 nm (red) and 550 nm (Green). Blue lines represent instrumental response functions (IRF). For (c), the emission lifetime is so long that the phosphorescence cannot decay enough. (d) The time range was extended up to 100 μs compared to (c) where the long-time component originated from phosphorescence.

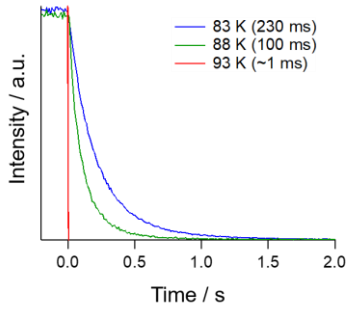

Fig. S12 Time resolved phosphorescence measurement from **[9]TH** in 2-Me-THF at 83 (blue), 88 (green), and 93 K (red). Evaluated phosphorescence lifetimes were shown in the parentheses.
If we assume that T_1 state only relaxes to S_0 through radiative k_p and non-radiative k_{nrp} pathways with Arrhenius formula, phosphorescence radiative rate constant is estimated as k_p~3 s^{-1}.

For time resolved phosphorescence measurement, 2-Me-THF solution of **[9]TH** was loaded in a liq-N_2 cryostat (CoolSpek Unisoku) and excited at 355 nm from CW Xe-lamp (LC8, Hamamatsu Photonics) through a band-pass filter. The phosphorescence decay was then detected by Si-APD (C16533, Hamamatsu Photonics) through a 550 nm band-pass filter and counted by universal frequency counter/timer (53230A, Keysight) with gate duration of 10 ms for 83, 88 K and 100 μs for 93 K.

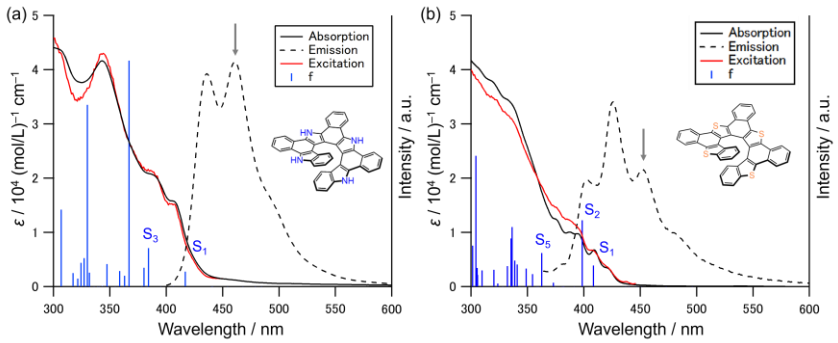

Fig. S13 Absorption (black solid), emission (black dotted), and excitation (red) spectra for (a) **[9]AH** and (b) **[9]TH** in CH_2Cl_2. The excitation wavelength for emission spectra was set to 380 (350) nm for **[9]AH** (**[9]TH**). The monitor wavelength for excitation spectra was set to 462 (452) nm for **[9]AH** (**[9]TH**) indicated as the arrows. The calculated oscillator strengths were also overlapped as blue bars (B3LYP/6-31G(d) level).

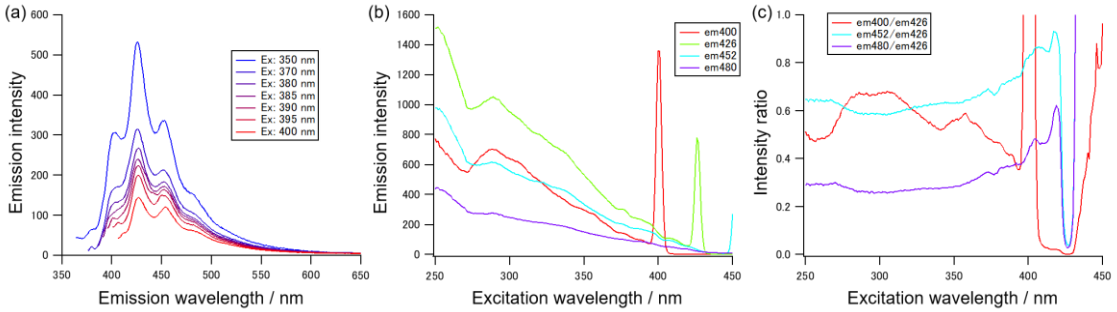

Fig. S14 (a) Emission spectra of **[9]TH** in dichloromethane (1 μM) excited at various wavelengths. (b) Excitation spectra for selected wavelengths at 400 (red), 426 (green), 452 (pale blue), and 480 nm (purple). The sharp peaks are due to the scattering of the excitation light. (c) Same as (b) but normalized by excitation spectra for 426 nm.

Excitation profile for **[9]TH** was studied more detail. Fig. S14(a) shows emission spectra of **[9]TH** in dichloromethane (1 μM) excited at various wavelength. Basically, four peaks were observed, namely, at 400, 426 (maxima), 452, and 480 nm (shoulder). We chose these four peaks as emission wavelengths and obtained excitation spectra as shown in Fig. S14(b). It is very clear from Fig. S14(b), the excitation spectra monitored at 400 nm is quite different from other three peaks, suggesting the excited state origin is different. For other three peaks, we have minor differences, e.g., the emission intensity at 452 nm and 426 nm are very close at excitation wavelength above 400 nm, but below 400 nm, emission at 452 nm is always lower than that at 426 nm. To see this effect more clearly, we took the emission intensity ratio between 400/452/480 nm v.s. 426 nm (Fig. S14(c)). First, the normalized excitation spectra at 452 nm and 480 nm are apparently in same trend, indicating these two originates sorely from S_1 state. Second, these two traces are not flat, indicating the emission at 426 nm contains different contribution from those at 452/480 nm. Finally, the emission at 400 nm decreases gradually above 360 nm. From these experiments, we consider that emission peaks at 452 and 480 nm mainly originated from S_1 state, and other two (400 and 426 nm) originated from S_1 and S_n states.

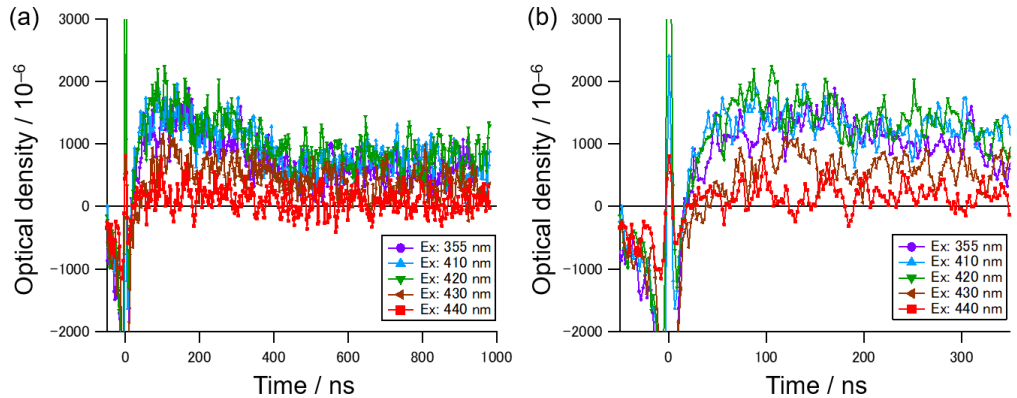

Fig. S15 (a) Nanosecond transient absorption kinetics of **[9]TH** solution (0.1 mM, CH_2Cl_2) at 450–550 nm. (b) Magnified view of (a).

Nanosecond TA study was approached by using streak camera system with a Nd:YAG OPO (resolution of ca. 6–7 ns in this time range). Transient absorption traces from **[9]TH** (0.1 mM in CH_2Cl_2) are plotted in Fig. S15 excited with variable wavelengths. Monitor wavelength was adjusted at ~500 nm where the triplet absorption appears. Although fluorescence artifact overlapped the transient spectra, transient kinetics were quite similar in 355, 410, and 420 nm excitation. On the other hand, the trace of 430 nm excitation delayed slightly from them. Although the resolution of Nd:YAG excitation pulse is not enough for detailed analysis, triplet generation from S_1 state would be slower than that from S_2 state.

6. Theoretical calculations

Ground and excited state geometry optimization was carried out by using Gaussian 16 code[1] with B3LYP functional and 6-31+G(d) basis set. Grimme's D3BJ (D3 with Becke-Johnson damping) dispersion correction[2] was adopted in the calculation. ECD spectra was simulated with same condition. Spin-orbit coupling matrix elements and excited state energy were estimated at geometrically relaxed state, using B3LYP functional and 6-31G(d) basis set with the ORCA-5.0.4 program[3] with Tamm-Dancoff approximation.

1. DFT calculations for [9]TH

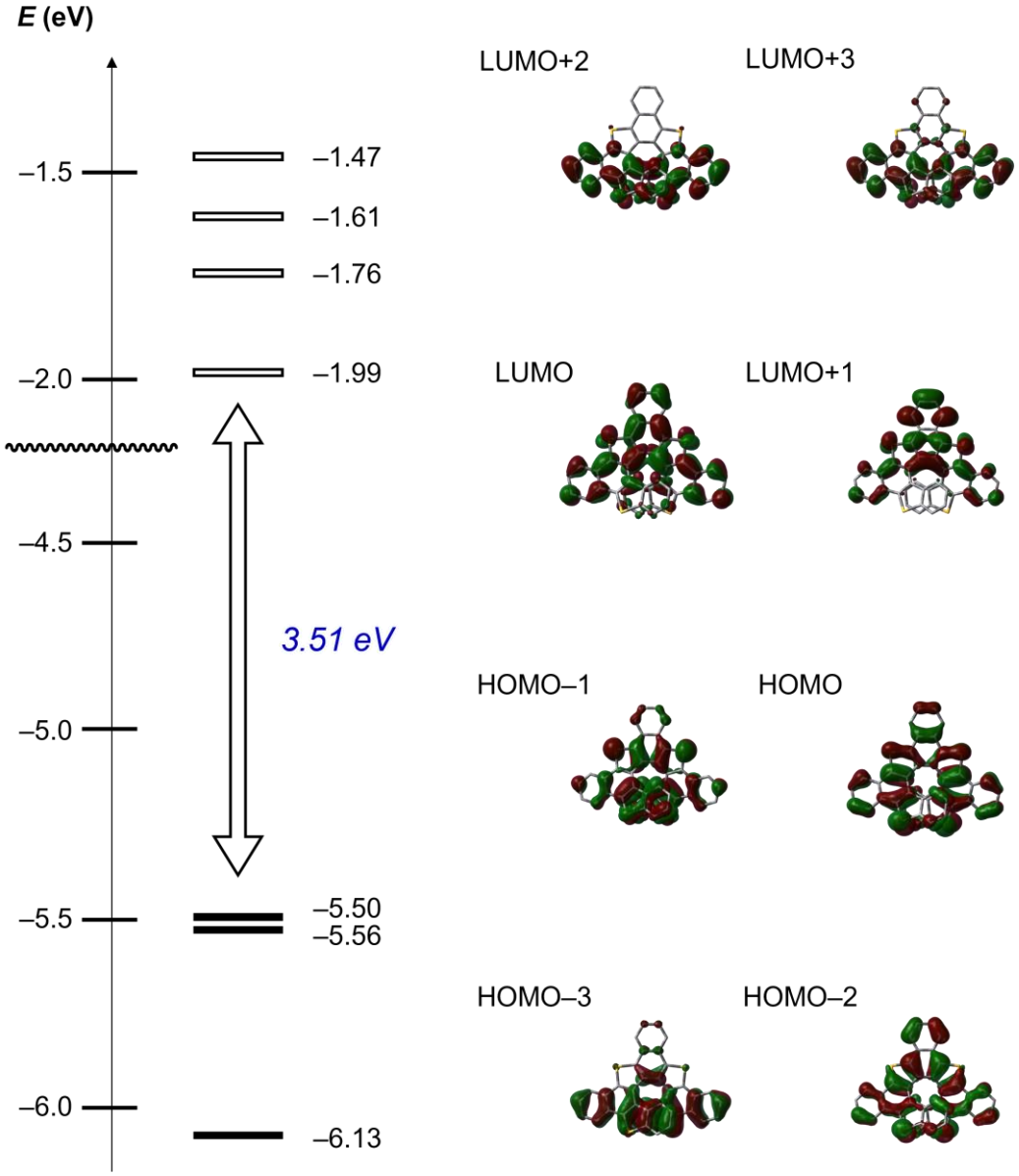

Fig. S16 Kohn–Sham MO representation and energy diagrams of **[9]TH** calculated at B3LYP/6-311G(d,p) level. Hydrogen atoms are omitted for clarity.

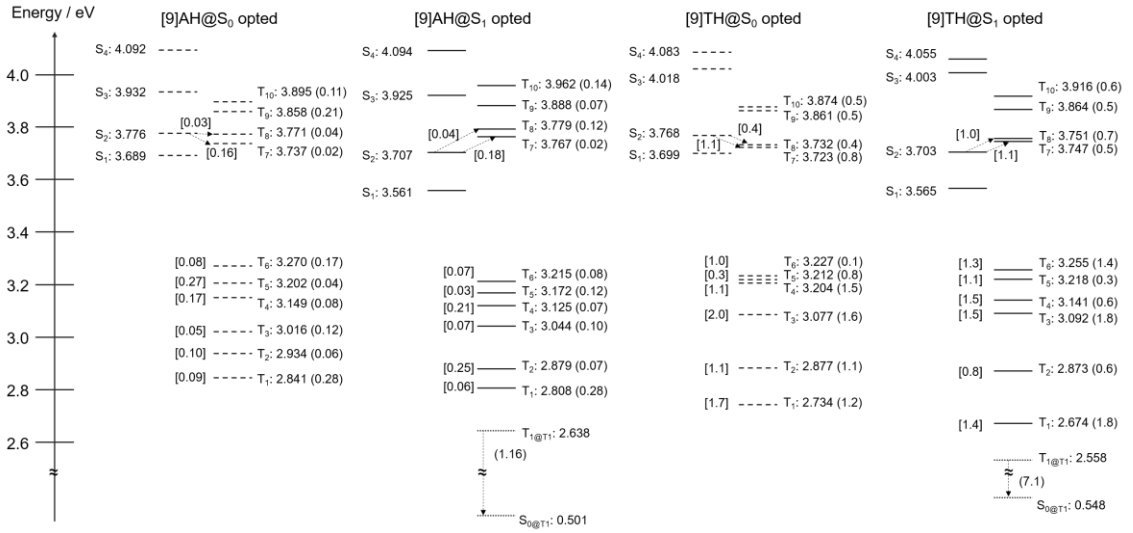

Fig. S17 Energy landscape for **[9]AH** and **[9]TH** calculated at CAM-B3LYP/6-31G(d) level. SOC constants were shown in the parentheses (S_1/T_n for S_1 and S_0 configuration, T_1/S_0 for T_1 configuration) or brackets (S_2/T_n) in cm^{-1}.

References

1. Gaussian 16, Revision C.01, M. J. Frisch, G. W. Trucks, H. B. Schlegel, G. E. Scuseria, M. A. Robb, J. R. Cheeseman, G. Scalmani, V. Barone, G. A. Petersson, H. Nakatsuji, X. Li, M. Caricato, A. V. Marenich, J. Bloino, B. G. Janesko, R. Gomperts, B. Mennucci, H. P. Hratchian, J. V. Ortiz, A. F. Izmaylov, J. L. Sonnenberg, D. Williams-Young, F. Ding, F. Lipparini, F. Egidi, J. Goings, B. Peng, A. Petrone, T. Henderson, D. Ranasinghe, V. G. Zakrzewski, J. Gao, N. Rega, G. Zheng, W. Liang, M. Hada, M. Ehara, K. Toyota, R. Fukuda, J. Hasegawa, M. Ishida, T. Nakajima, Y. Honda, O. Kitao, H. Nakai, T. Vreven, K. Throssell, J. A. Montgomery, Jr., J. E. Peralta, F. Ogliaro, M. J. Bearpark, J. J. Heyd, E. N. Brothers, K. N. Kudin, V. N. Staroverov, T. A. Keith, R. Kobayashi, J. Normand, K. Raghavachari, A. P. Rendell, J. C. Burant, S. S. Iyengar, J. Tomasi, M. Cossi, J. M. Millam, M. Klene, C. Adamo, R. Cammi, J. W. Ochterski, R. L. Martin, K. Morokuma, O. Farkas, J. B. Foresman, and D. J. Fox, Gaussian, Inc., Wallingford CT, **2016**.

2. S. Grimme, *J. Comput. Chem.* **2006**, *27*, 1787–1799., S. Grimme, J. Antony, S. Ehrlich and H. Krieg, *J. Chem. Phys.* **2010**, *132*, 154104., S. Grimme, S. Ehrlich and L. Goerigk, *J. Comput. Chem.* **2011**, *32*, 1456–1465.

3. Neese, F. *Wiley Interdisciplinary Reviews - Computational Molecular Science*, **2012**, *2*, 73–78.